

Numerical analysis of superscatterer applied in inductive coupling system to equivalently expand and move coils

Yingyi Zhang¹ · Xudong Luo² · Chen Yao¹ · Yuncheng Li¹ · Houjun Tang¹

Received: 23 March 2015 / Accepted: 7 August 2015 / Published online: 22 August 2015
© Springer-Verlag Berlin Heidelberg 2015

Abstract Superscatterer is typically made of complementary media for expanding the scope of scattering. The fact that superscatterer can make object appear bigger than its geometric size provides the possibility of equivalently enlarging and moving coils in inductive coupling system. In this paper, we demonstrate that the superscatterer without perfect electrical conductor can also expand the distribution of magnetic field with a source inside. Based on transformation optics, a spherical superscatterer is designed and simulated especially in near field. A model of two-coil inductive coupling system is numerically analyzed to prove the enhancement on mutual coupling by superscatterer. Finally, we also discuss the simplification of such superscatterer for fabrication concerns.

1 Introduction

In order to manipulate electromagnetic (EM) field from optical frequency down to DC, electromagnetic metamaterial was proposed as a new paradigm to design EM devices [1]. Based on the methodology of coordinate transformation [2], novel applications such as invisible cloak [3], EM rotators [4] and planar focusing antennas [5] were theoretically predicted and experimentally verified at

microwave frequency [6]. Compared with invisible cloak which attempts to reduce all the scattering and hide the inner object in EM radiation, traditional superscatterer is designed to expand the scope of scattering and to make EM detection larger than the actual size of object [7]. With the existence of superscatterer, light ray is bounced back on the virtual surface making the scattering field nearly identical to that of a real bigger object. This phenomenon has already been applied to conceal entrance [8] and shrink optical device [9] in previous work. In this paper, it will be utilized to expand and move coils.

According to the transformation optics and concept of complementary media, the superscatterer could be achieved by perfect electrical conductor (PEC) and negative index material (NIM) [10]. The NIM was always composed of metamaterials whose permittivity and permeability were both negative [11]. In the past few years, various metamaterials with negative EM parameters have been designed at megahertz [12], which made their applications possible in wireless power transfer (WPT) or energy harvest system [13]. However, most of WPT systems [14] with metamaterials were based on the effect of negative refraction and evanescent wave amplification [15]. In these cases, the effective permeability of metamaterials was always selected as -1 due to the theory of ‘Magnetic Super-Lens’ [16]. In this respect, a thicker metamaterial slab would be needed if a longer transmission distance was required. Furthermore, the metamaterials in previous cases were shaped into rectangular solid and placed in the middle position of two-coil system, which occupied more space and was a sort of cumbersome.

Here, we provide a spherical shell of superscatterer without PEC boundary enclosing transmitting or receiving coil in inductive coupling system. We also exhibit its enhancement on mutual coupling and its advantages compared with

✉ Yingyi Zhang
zhangyingyi@sytu.edu.cn

¹ Key Laboratory of Control of Power Transmission and Transformation Ministry of Education, 800 Dongchuan RD., 200240 Shanghai, China

² Department of Physics and Astronomy, Key Laboratory of Artificial Structures and Quantum Control (Ministry of Education), Shanghai Jiao Tong University, Shanghai 200240, China

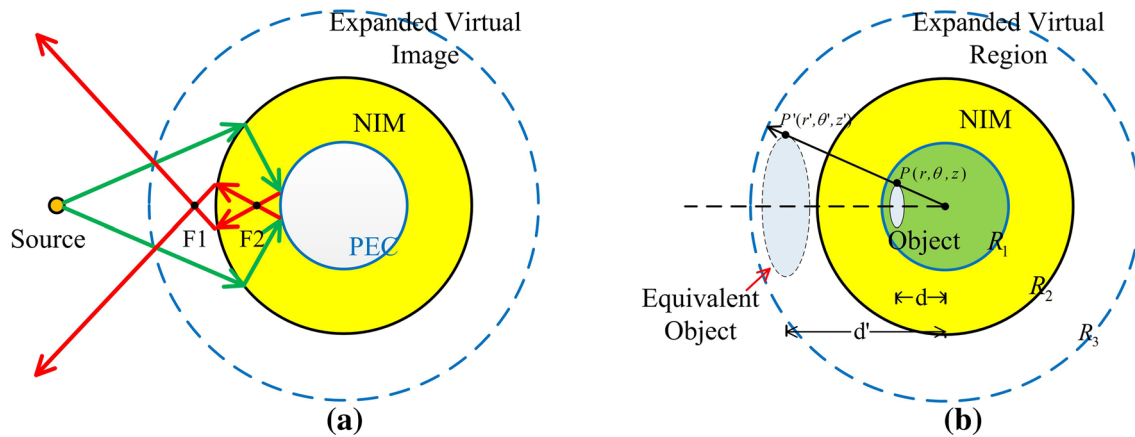


Fig. 1 **a** Typical superscatterer with PEC. **b** Superscatterer without PEC applied in coil system

those in previous cases. Theoretical and systematic models of superscatterer are numerically analyzed to evaluate its performance on mutual inductance, quality factor and enhanced efficiency ratio.

2 Analysis of superscatterer without PEC boundary

Complementary media theory [17] indicates that if properties of two media are anti-symmetrical relative to a surface, they could be removed equivalently in optics. Hence, the boundary on one side, usually PEC boundary, seemed to be moved onto the other side, which was the principle of a typical cylindrical superscatterer displayed in Fig. 1a. In contrast to the typical superscatterer including PEC boundary with a source outside [18], the superscatterer applied in magnetic coupling system is required to encircle the source coil. In this case, PEC boundary should be removed and new media should be filled in the region around source to create an equivalent enlarging effect of the coil. The schematic plot of cylindrical superscatterer without PEC boundary is displayed in Fig. 1b.

In Fig. 1b, the EM media in region $r < R_1$ should reconstruct the entire EM field in region $r < R_3$ because the complementary media in region $R_1 < r < R_2$ and $R_2 < r < R_3$ have mutually counteracted. From a material perspective, the media in $r < R_1$ is expanded from boundary R_1 to the blue dash line, which can simultaneously enlarge and move the image of object embedded in the media. For analysis, a cylindrical coordinate is set up with origin at the center and z -axis perpendicular to the plane. The transformation equation in $r < R_1$ can be written as follows:

$$r' = (R_3/R_1)r, \theta' = \theta, z' = z \quad (1)$$

Here, r', θ', z' are the parameters of virtual transformed region $r < R_3$, which is enclosed by blue dash line. Based

on transformation optics [19], r, θ, z denoting parameters in physical region $r < R_1$ can be derived from r', θ', z' . The tensor of permittivity and permeability of media in $r < R_1$ can be obtained (see Eq. (2)) by transformation in orthogonal coordinates [20].

$$\varepsilon_r^{(r,\theta,z)} = \mu_r^{(r,\theta,z)} = \begin{bmatrix} 1 & 0 & 0 \\ 0 & 1 & 0 \\ 0 & 0 & (R_3/R_1)^2 \end{bmatrix} \quad (2)$$

As for the region $R_1 < r < R_2$, the same way as typical superscatterer, media filled in this area should counteract the empty space in $R_2 < r < R_3$. The transformation equations for these complementary media are written in Eq. (3).

$$r' = \frac{R_2 - R_3}{R_2 - R_1}r + \frac{R_3 - R_1}{R_2 - R_1}R_2, \theta' = \theta, z' = z \quad (3)$$

After transformation, the boundary $r = R_1$ is mapped to boundary $r < R_3$, which means the region $R_1 < r < R_3$ has been folded in half along the boundary $r = R_2$. The NIM metamaterials inevitably appear in region $R_1 < r < R_2$ due to folded geometry [21], which is reflected by negative EM parameters in tensor.

$$\varepsilon_r^{(r,\theta,z)} = \mu_r^{(r,\theta,z)} = \begin{bmatrix} \frac{rb-cR_2}{rb} & 0 & 0 \\ 0 & \frac{rb}{rb-cR_2} & 0 \\ 0 & 0 & \frac{rb^2-bcR_2}{ra^2} \end{bmatrix} \quad (4)$$

Here, $a = R_2 - R_1$, $b = R_3 - R_2$, and $c = R_3 - R_1$. The equivalent effect of superscatterer is that the inside object becomes R_3/R_1 times larger than itself and the distance from object to center becomes R_3/R_1 times longer than original one. To verify it, a 2D model is established with different media derived from Eq. (2) and (4) in COMSOL MULTIPHYSICS. The detailed parameters are set as: $R_1 = 0.5$ m, $R_2 = 1$ m, $R_3 = 2$ m. The internal line source with a radius $R_c = 0.1$ m is

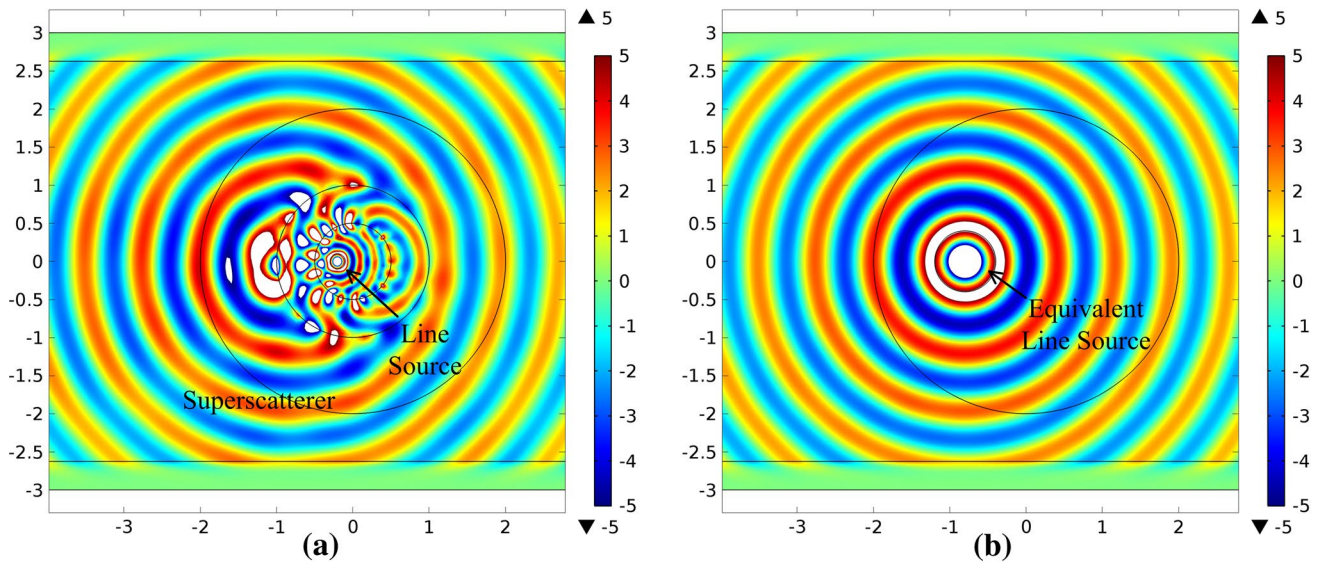


Fig. 2 The distribution of electric field with a line source. **a** Line source with superscatterer. **b** Equivalent larger and shifted line source without superscatterer

placed 0.2 m away from the center. A 400-MHz current is added on the line source. For comparison, the model with equivalent line source is set up and excited by same frequency current, which has a radius $R_c = 0.4$ m and a 0.8-m displacement. The corresponding EM fields are displayed in Fig. 2.

As depicted in Fig. 2a, b, the EM field (outside the superscatterer) of original source is nearly identical to that of a larger and shifted equivalent line excitation. We can conclude that by using superscatterer without PEC boundary, the EM field of an internal source can be equivalently expanded to any size and moved to corresponding position.

3 Superscatterer applied in inductive coupling system

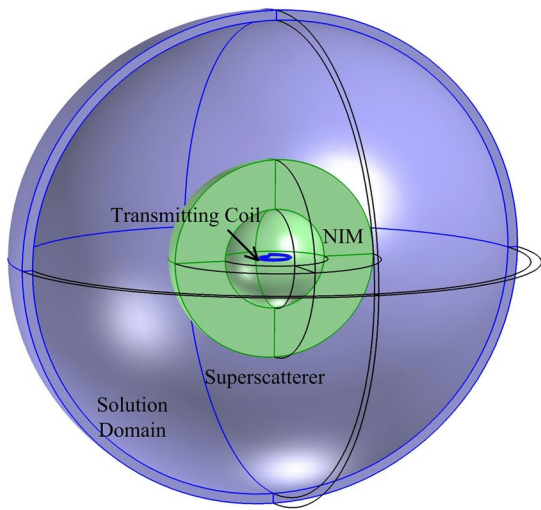
Next, let us discuss another interesting topic: What if the excitation in superscatterer is transmitting or receiving coil working at relatively low frequency? In order to evaluate the performance of superscatterer in near field, three models of transmitting coil are built and simulated, respectively, in Fig. 3 for comparison. In Fig. 3a, the transmitting coil has 0.15 m radius and 2 mm radius of cross section and is excited by 2A current at 10 MHz. The coil is encompassed by a spherical shell of superscatterer with the radii $R_1 = 0.5$ m, $R_2 = 1$ m, $R_3 = 2$ m. The coil is placed 0.3 m away from the center of sphere. By coordinate transformation, the permittivity and permeability tensors of media in region $r < R_1$ and $R_1 < r < R_2$ are written in Eqs. (5) and (6).

$$\epsilon_r^{(r,\theta,\varphi)} = \mu_r^{(r,\theta,\varphi)} = \begin{bmatrix} R_3/R_1 & 0 & 0 \\ 0 & R_3/R_1 & 0 \\ 0 & 0 & R_3/R_1 \end{bmatrix} \quad (5)$$

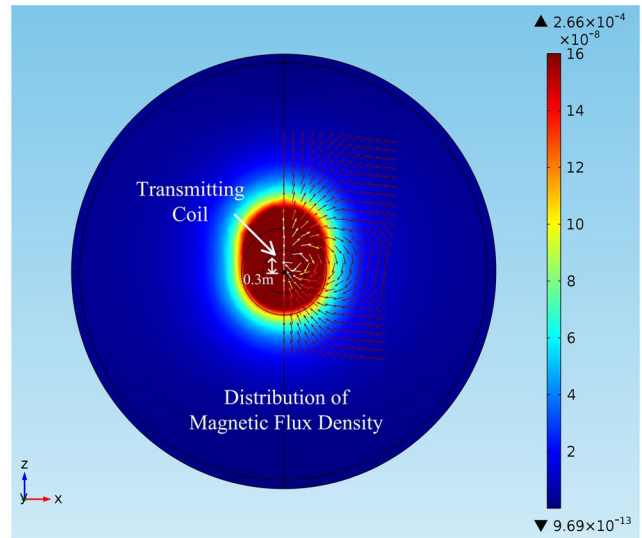
$$\epsilon_r^{(r,\theta,\varphi)} = \mu_r^{(r,\theta,\varphi)} = \begin{bmatrix} \frac{R_1-R_2}{R_3-R_2} \cdot \frac{r^2}{r^2} & 0 & 0 \\ 0 & \frac{R_3-R_2}{R_1-R_2} & 0 \\ 0 & 0 & \frac{R_3-R_2}{R_1-R_2} \end{bmatrix} \quad (6)$$

The tensor in Eq. (5) indicates that the media in region $r < R_1$ are isotropic and homogeneous with positive value which is easy for fabrication. In region $R_1 < r < R_2$, however, media are anisotropic with negative value. To reduce the difficulty of designing metamaterials with negative value, we assume that: $\epsilon_r = 1$ in subsequent models and μ_r is still derived from Eqs. (5) and (6). Considering the electric and magnetic fields are mostly decoupled in near field [12] and we primarily focus on the magnetic flux distribution [14], this assumption of only negative permeability is reasonable to evaluate the performance of superscatterer and influence of impedance mismatch. By numerical simulation, the magnetic flux density distribution of superscatterer is plotted in Fig. 3c. The brighter color denotes the higher value.

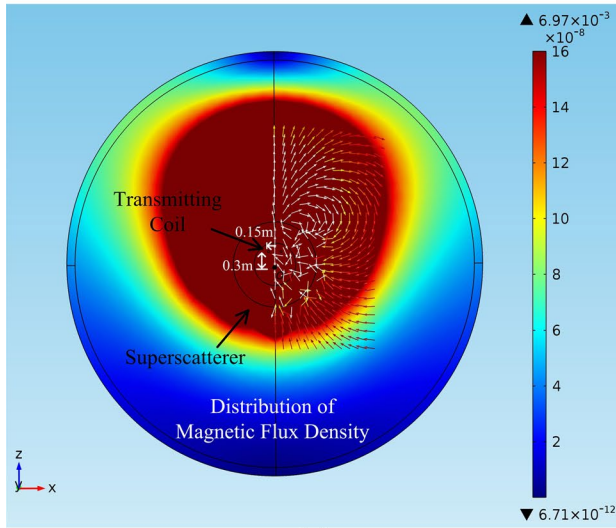
Another three models are also discussed in Fig. 3, and source current in all models is 2A at 10 MHz. Firstly, a same transmitting coil without superscatterer is simulated whose magnetic flux density is depicted in Fig. 3b. Secondly, a transmitting coil with 0.6 m radius (derived from $(R_3/R_1) \cdot 0.15$ [m]) and 8 mm radius of cross section is placed 1.2 m away from the center. Figure 3d shows its



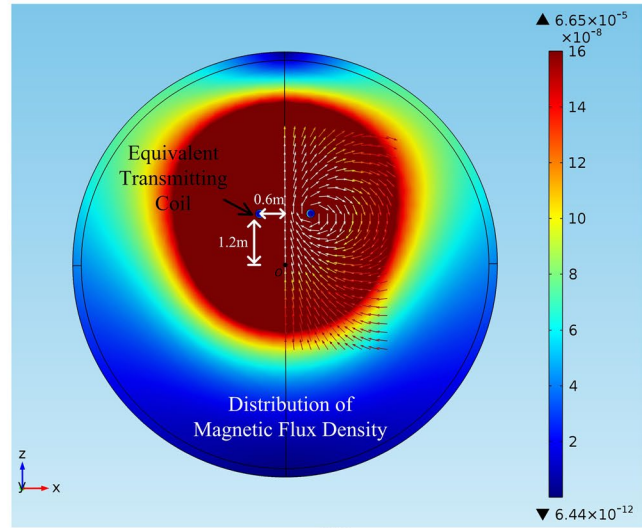
(a)



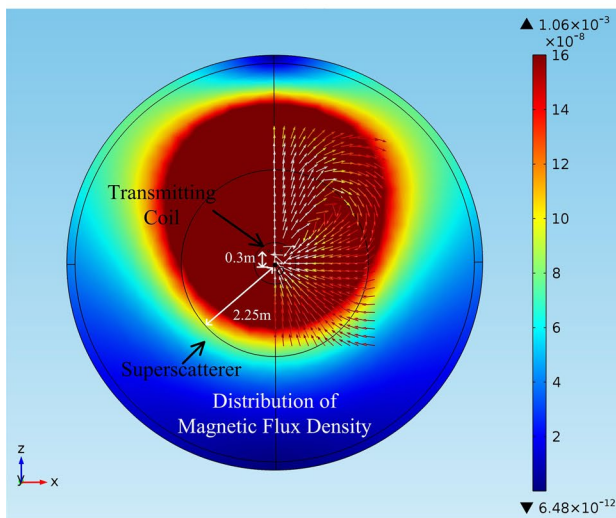
(b)



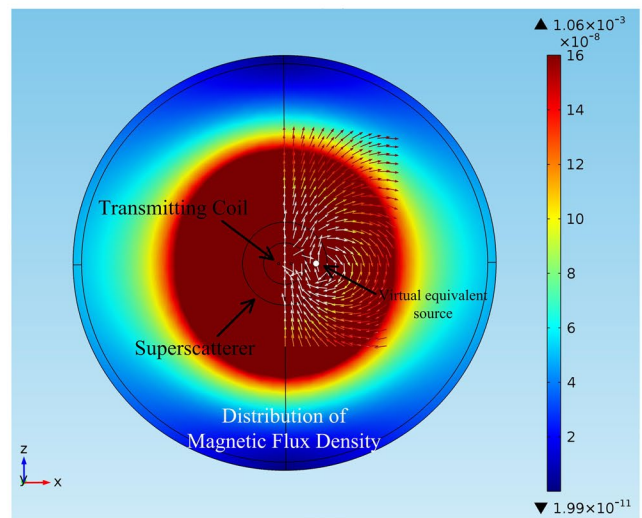
(c)



(d)



(e)



(f)

Fig. 3 **a** The simulation model of transmitting coil with superscatterer. The magnetic flux density of **b** original transmitting coil without superscatterer, **c** transmitting coil with superscatterer, **d** equivalent larger and shifted transmitting coil. **e** The magnetic flux density of superscatterer without complementary media. **f** The magnetic flux density of coil at the center of superscatterer

distribution of magnetic flux density under the same scale. Thirdly, the initial transmitting coil is placed exactly at the center of sphere coated by superscatterer, and its result is displayed in Fig. 3f. Obviously, the magnetic field in Fig. 3c, d is nearly the same, which means transmitting coil with superscatterer can approximately act like a four times larger coil and move farther even in near field. If the coil is placed at the center without displacement, the equivalent coil will not move but the expansion effect still holds (see Fig. 3f). In a word, mutual coupling in two-coil system will definitely be enhanced if transmitting or receiving coil can be enlarged four times or more.

In addition, superscatterer without using complementary media is proposed in previous work [22]. In Ref [22], similarly, the inner radius is expanded, but the virtual enlarged boundary is still confined inside the outer radius. Meanwhile, the initial outer shell is compressed into a thinner layer without being folded. Hence, the negative material can be avoided. To make some comparison, a superscatterer based on Ref [22] is set up in Fig. 3e with inner radius $R_1 = 0.5\text{ m}$ and outer radius $R_2 = 2.25\text{ m}$. The initial coil is still placed 0.3 m away from center, and such device is also designed to expand the coil four times larger. According to Fig. 3e, the magnetic field is nearly the same as that in Fig. 3c, d, which proves the validity and equivalence of two kinds of superscatterer.

In Fig. 3c, d, the equivalent larger coil is moved to the position 1.2 m away from center, which is outside the

superscatterer. As for Fig. 3e, however, the expanded and shifted coil is still confined in the superscatterer without NIM. That is, to enlarge the coil, such superscatterer should be even larger than the equivalent coil to coat it, which increases the fabrication cost and the space it takes up. Clearly, the superscatterer in Fig. 3e is more cumbersome than that in Fig. 3c. The latter superscatterer is more suitable for coupling system and other wireless transmission systems because it is more compact.

To verify the performance of superscatterer in Fig. 3c, a practical inductive coupling system with high-frequency inverter and a load of $1\text{ k}\Omega$ is discussed (see Fig. 4). The high-frequency inverter is working at 10 MHz which is feasible for RF MOSFET. The transmitting coil is excited by 2 A current at 10 MHz . The geometric parameters of coil and superscatterer are the same as those in Fig. 3a. Moreover, a receiving coil with 0.5 m radius and 2 mm radius of cross section is placed 2.5 m away from source coil. The two coils are coaxial and displayed under an axisymmetric 2D view in Fig. 4b. A spherical coordinate system with origin at the center of sphere is set up for simulation.

Similarly, another two models of inductive coupling system are built for comparison. They are: the model of original same coils and the model of equivalent larger and shifted source coil. Both of them have no superscatterers. To demonstrate the displacement effect by superscatterer, the distance between transmitting coil and center of sphere is swept from 0 to 0.34 m in all models. That means the transmitting coil is moving closer to the shell of superscatterer. From an engineering point of view, the assessment of entire system mainly focuses on mutual inductance M , quality factor Q and enhanced efficiency ratio $\eta_{enhance}$, which are computed by Eq. (7) and depicted in Fig. 5 under three circumstances. Here, V_2 denotes the voltage of receiving coil. I_1 is the excitation current on transmitting coil. ω

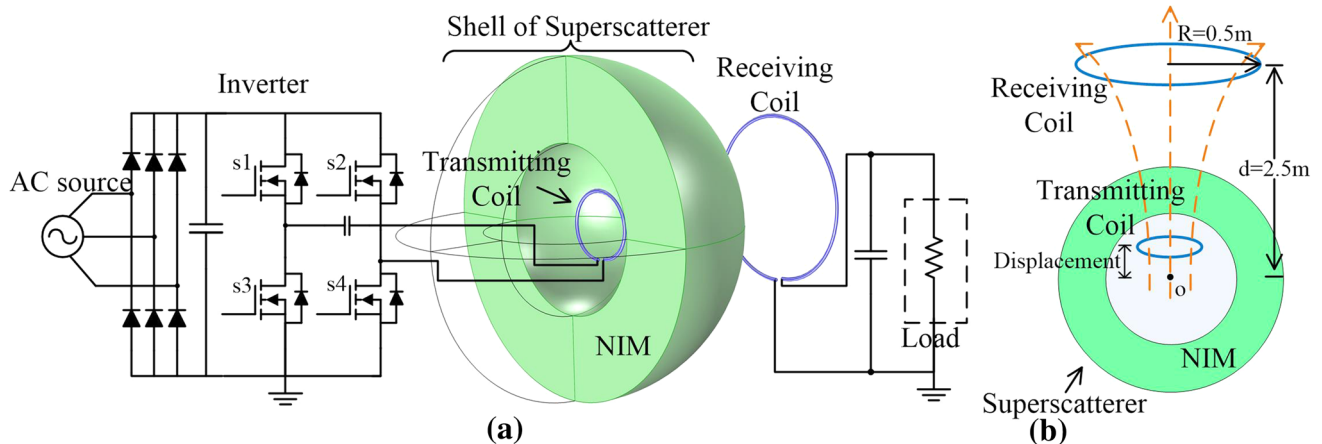


Fig. 4 **a** The inductive coupling system including inverter, superscatterer, coils and load. **b** The simplified system with two coils and superscatterer under the axisymmetric 2D view

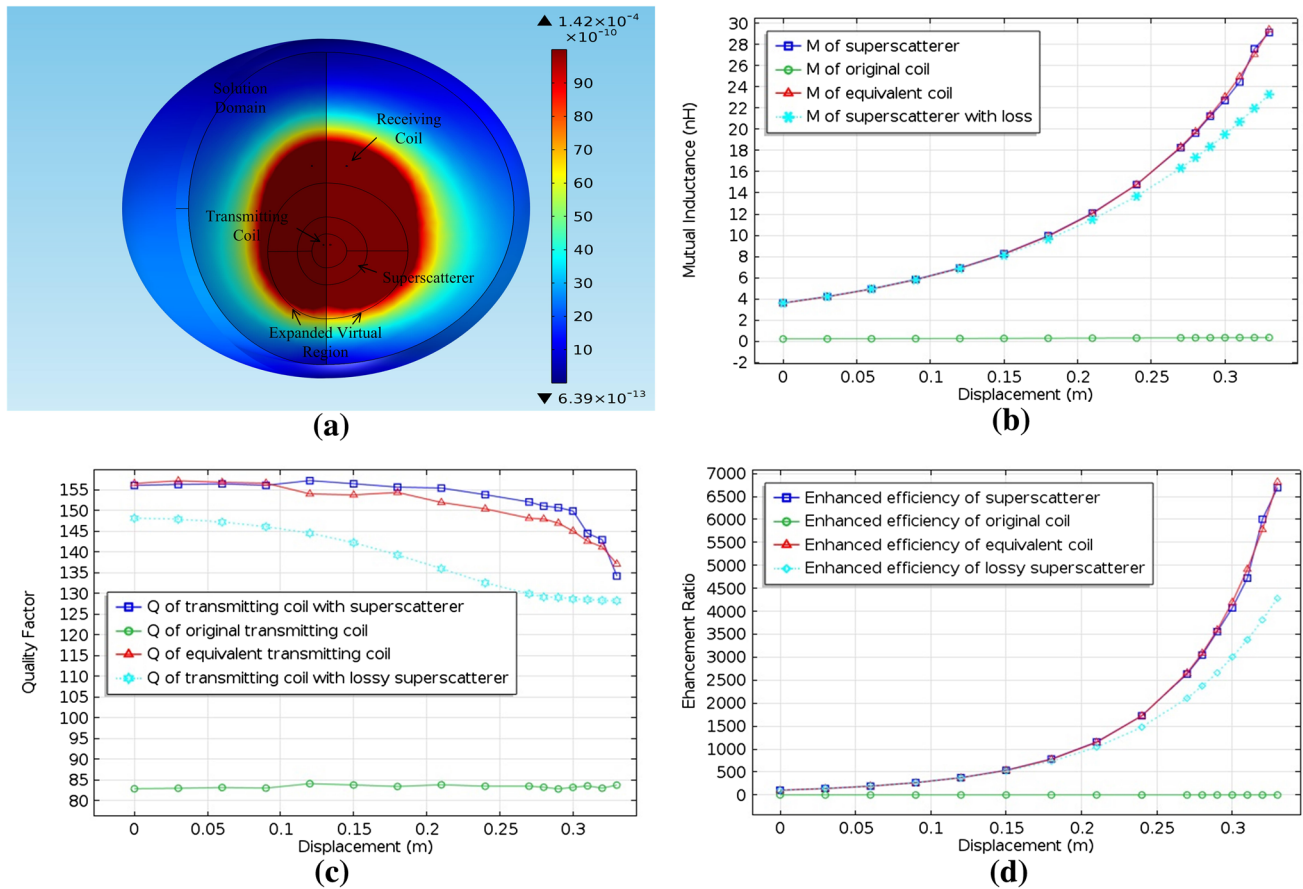


Fig. 5 **a** Snapshot of the magnetic flux density of a coupling system. The transmitting coil is enclosed by superscatterer with a 0.21-m displacement from the center of sphere. **b** Mutual inductance, **c** quality factor of transmitting coil, **d** enhanced efficiency ratio in different cases

is the angular frequency of high-frequency inverter. L_1 and r_1 are self-inductance and resistance of transmitting coil separately. η_{with} denotes efficiency measured in three cases, and $\eta_{without}$ specifically denotes efficiency measured with original coils.

$$M = \frac{V_2}{j\omega \cdot I_1}, \quad Q = \frac{\omega L_1}{r_1}, \quad \eta_{with,without} = \frac{P_{load}}{P_{input}}, \quad \eta_{enhance} = \frac{\eta_{with}}{\eta_{without}} \quad (7)$$

To compute M , the receiving coil is set as open circuit with no load and V_2 is open-circuit voltage of receiving coil which can be derived from coil parameters in COMSOL. To evaluate Q and power, the load (as circuit component) is added into the model using nodes to be connected with receiving coil. Both EM field and circuits should be computed simultaneously. Also, the self-inductance and self-resistance can be derived from coil parameters in global evaluation in COMSOL. Since the load and receiving coil are connected in series, the current in coil can be used to compute the power: $P_{load} = (I_2)^2 R_d$. Here, I_2 is induced current in receiving coil (also passes through the load)

and R_d denotes the load value, which is 1 k Ω in this case. Again, current I_2 can be derived from coil parameter of receiving coil.

Figure 5a exhibits the distribution of magnetic flux density with superscatterer at source coil, which is significantly expanded and moved closer to receiving coil by superscatterer. Figure 5b shows the curves of mutual inductance changing with distance. We can find that mutual inductance of system with superscatterer increases dramatically and is much bigger than that with nothing. Furthermore, the result of coil with superscatterer agrees pretty well with that of equivalent larger and shifted coil. In Fig. 5c, d, similarly, the quality factor of transmitting coil and enhanced efficiency ratio with superscatterer give a much better performance than that with nothing and highly match the performance of equivalent source coil. In engineering interpretation, the higher mutual inductance promises stronger magnetic coupling of two-coil system. The higher quality factor brings lower dissipation loss and better frequency selectivity. The enhanced efficiency ratio affected by mutual inductance and quality factor is definitely the significant indicator of practical application. To sum up,

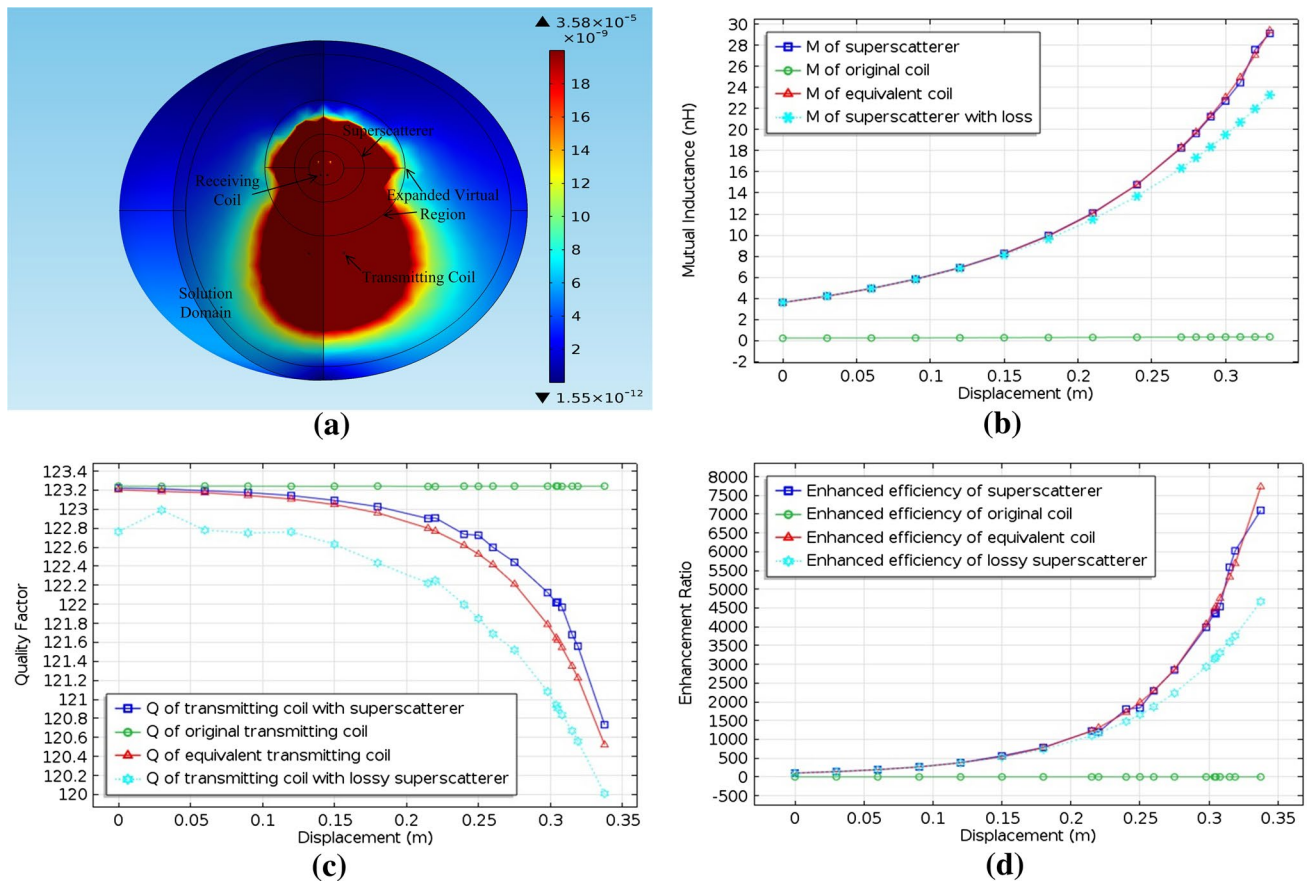


Fig. 6 **a** Snapshot of the magnetic flux density of a coupling system. The receiving coil is enclosed by superscatterer and has a 0.21-m displacement from the center of sphere. **b** Mutual inductance, **c** quality factor of transmitting coil, **d** enhanced efficiency ratio in different cases

the enhancement is partly attributed to the expanded size of coil which is reflected by increased self-inductance and is partly attributed to shifted position of coil which is verified by sharp increment on mutual inductance and efficiency. In this respect, the effects of the coil with superscatterer and those of a larger and shifted coil are nearly equivalent. That is, we can enlarge the transmitting coil and shift it to a desired position by proposed superscatterer.

$$\begin{aligned} \varepsilon &= \varepsilon' - j\left(\varepsilon'' + \frac{\sigma}{\omega}\right) \\ \mu &= \mu' - j\mu'' \end{aligned} \tag{8}$$

As for practical metamaterials, both magnetic loss and ohmic loss should be considered. In general, the complex permittivity and permeability are written in Eq. (8). The imaginary part of permeability reflects the magnetic loss. The imaginary part of permittivity indicates both polarization loss and ohmic loss. To evaluate superscatterer with loss, we use $\varepsilon_r = 1 \cdot (1 - j \cdot \sigma_1)$ and $\mu_r = -\mu' \cdot (1 + j \cdot \sigma_2)$ to mimic the superscatterer with loss. Here, σ_1, σ_2 are dielectric loss tangent and magnetic loss tangent, respectively. In this model, we set $\sigma_1 = 0.0025$ which is slightly more

than that of substrate material Rogers6010 and $\sigma_2 = 0.025$ which is the same as loss tangent in previous work [16]. By repeating the computation, the curves of M , Q and $\eta_{enhance}$ are plotted in Fig. 5 with cyan dotted line. Compared with ideal device, the performance of lossy superscatterer decreases, but it is still much better than that of original system.

Correspondingly, the models of superscatterer enclosing receiving coil are simulated in Fig. 6. The conditions of three models are identical to those in Fig. 5. In this part, original transmitter acts as receiver and original receiver serves as transmitter (see Fig. 6a). The curves of mutual inductance, quality factor of transmitting coil and enhanced efficiency ratio are depicted in Fig. 6b–d, respectively. Moreover, magnetic loss and ohmic loss are also considered and evaluated in cyan dotted line (the loss tangents σ_1, σ_2 are the same as those in Fig. 5). The results indicate that curves of ideal superscatterer and equivalent case are in good agreement and the mutual coupling and efficiency are still significantly enhanced by superscatterer with loss. However, the quality factor of transmitting coil does not increase (actually has a slight drop) because the

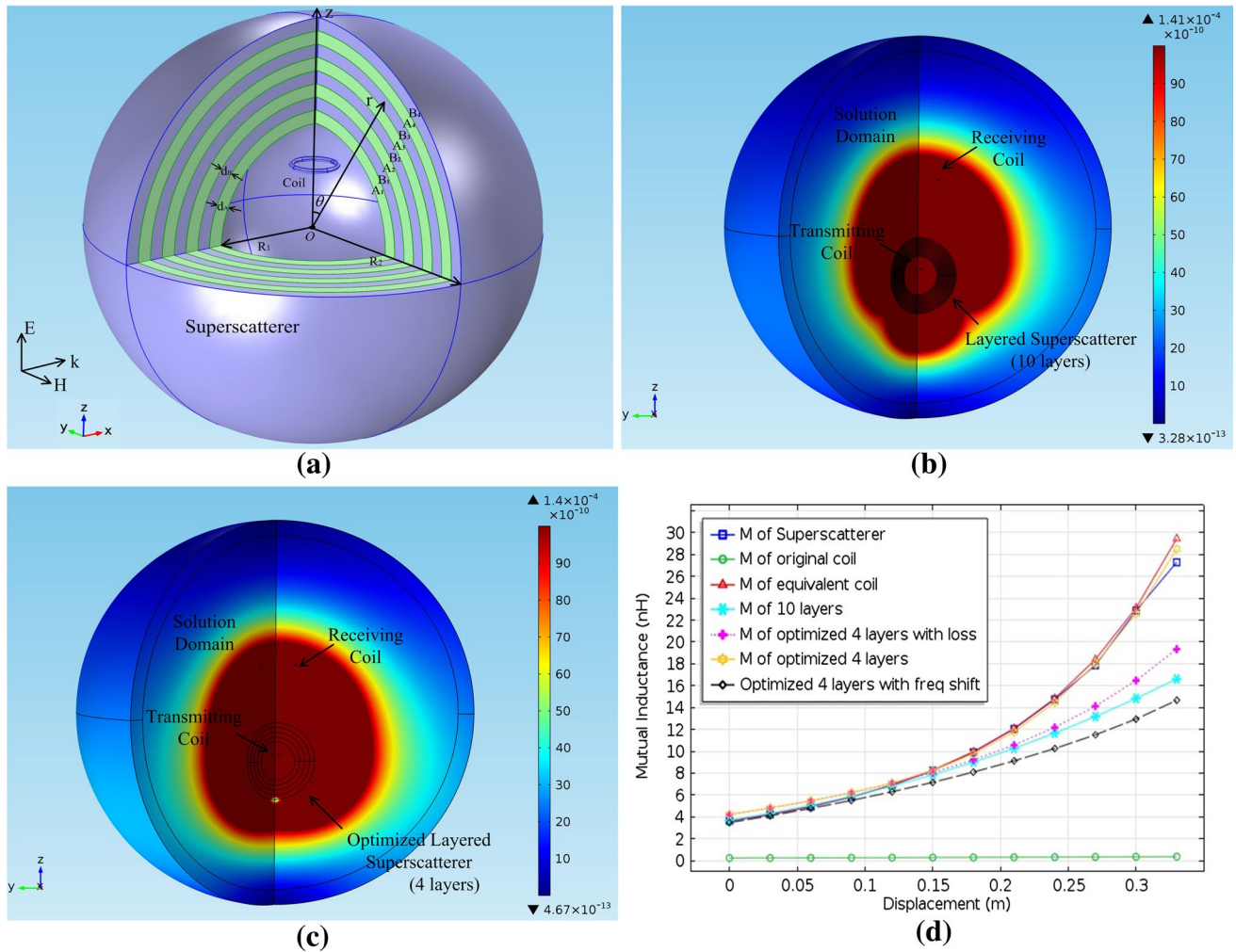


Fig. 7 **a** 3D structure of layered superscatterer. **b** Magnetic flux density of 10-layered superscatterer. **c** Magnetic flux density of optimized 4-layered superscatterer. **d** Mutual inductance in different cases

superscatterer enclosing the receiving coil does not enlarge the transmitting coil and affects the self-inductance of transmitting coil.

Compared with previous work on metamaterials in inductive coupling system [14], superscatterer without PEC boundary can expand the coils to desired size and move them to a farther position by altering the EM parameters of media. In other words, unlike the thick metamaterial slab in WPT system or other superscatterer without NIM, this superscatterer device need not be thicker or larger for a longer transmission distance.

4 Simplification of superscatterer

In Eq. (5), the material in region $r < R_1$ is homogeneous and isotropic with positive permittivity and permeability, which is feasible for fabrication. Although media in

region $R_1 < r < R_2$ are anisotropic and inhomogeneous material, they can be approximately obtained by layered structure of homogeneous and isotropic materials [23]. As electric field and magnetic field are decoupled in near field and most current WPT systems are based on magnetic coupling, we set $\epsilon_r = 1$ and mainly focus on permeability in the following discussion. In this part, we still use the same superscatterer model in Sect. 3 with radii $R_1 = 0.5$ m, $R_2 = 1$ m, $R_3 = 2$ m to illustrate the simplification process.

In Fig. 7a, superscatterer in $R_1 < r < R_2$ is equally divided into several concentric layers with homogeneous and anisotropic materials. Each layer is then alternately segmented into isotropic sublayer A and sublayer B. By effective medium theory (EMT), the permeability of each layer can be presented (Eq. 9), and η denotes the thickness quotient of two sublayers. This is the most common way to simplify anisotropic materials in previous papers [23, 24].

Table 1 Permeability of 10-layered superscatterer ($d_A = d_B = 0.025\text{m}$ for each layer)

Layer	Layer 1	Layer 2	Layer 3	Layer 4	Layer 5
μ_A	$-2.00 - 3.13i$	$-2.00 - 2.52i$	$-2.00 - 1.96i$	$-2.00 - 1.40i$	$-2.00 - 0.76i$
μ_B	$-2.00 + 3.13i$	$-2.00 + 2.52i$	$-2.00 + 1.96i$	$-2.00 + 1.40i$	$-2.00 + 0.76i$
Layer	Layer 6	Layer 7	Layer 8	Layer 9	Layer 10
μ_A	-2.71	-3.15	-3.40	-3.57	-3.69
μ_B	-1.29	-0.85	-0.60	-0.43	-0.31

$$\mu_\theta = \frac{\mu_A + \eta\mu_B}{1 + \eta}, \quad \frac{1}{\mu_r} = \frac{1}{1 + \eta} \left(\frac{1}{\mu_A} + \frac{\eta}{\mu_B} \right), \quad \eta = \frac{d_B}{d_A} \tag{9}$$

For example, 10-layered structure and $\eta = 1$ are selected, which means same thickness is assigned to sublayers A and B in each layer. Compared with EM wavelength, the layers are thin enough to mimic the superscatterer shell. By Eq. (9), permeability of each layer is computed and listed in Table 1. The permeability is then taken into each layer for numerical analysis. As a result, the magnetic flux density of 10-layered superscatterer is displayed in Fig. 7b and mutual inductance of coupling system is evaluated in cyan line with asterisk marker (see Fig. 7d. Admittedly, the performance of 10-layered superscatterer relatively declines due to finite number of layers. However, the effects of expansion and displacement still hold and mutual inductance with layered superscatterer can still outstrip that of initial system with nothing. For fabrication concerns, permeability parameters in Table 1 are with limited negative value which are possible for resonant metamaterials (such as split ring resonator). However, the disadvantages of this method are also very obvious: Firstly, several parameters exhibit negative imaginary part which means magnetic gain from passive materials. To overcome this, active materials or extra energy should be added into system which is not practical for most inductive coupling applications. Secondly, layer number should be increased to achieve a better approximation, which increases the difficulty and cost of fabrication.

Enlightened by optimization of cylindrical cloak with limited number of layers [25], we use similar approach to reduce the complexity of spherical superscatterer and its fabrication. Since we only need to simplify the superscatterer shell in $R_1 < r < R_2$, this situation is same with layering on typical superscatterer with PEC boundary. This problem can be solved by Mie scattering theory.

We suppose that an incident TE plane wave is propagating along x axis and the electric field is in z direction (see Fig. 7a). To employ Mie scattering theory in spherical coordinate system, we introduce Hertzian vectors of both electric and magnetic fields. The incident component of EM

field can be written as follows in forms of Bessel function of the first kind.

$$\prod_e^i = j \frac{\cos \varphi}{k^2} \sum_{n=1}^\infty a_n j^{-n} \hat{J}_n(kr) P_n^1(\cos \theta)$$

$$\prod_m^i = j \frac{\sin \varphi}{k^2 Z} \sum_{n=1}^\infty d_n j^{-n} \hat{J}_n(kr) P_n^1(\cos \theta) \tag{10}$$

Here, $P_n^1(\cos \theta)$ is the associated Legendre polynomials. The scattering field in superscatterer shell can be expanded as a sum of Hankel function of the second kind:

$$\prod_e^s = j \frac{\cos \varphi}{k^2} \sum_{n=1}^\infty b_n j^{-n} \hat{H}_n^{(2)}(kr) P_n^1(\cos \theta)$$

$$\prod_m^s = j \frac{\sin \varphi}{k^2 Z} \sum_{n=1}^\infty c_n j^{-n} \hat{H}_n^{(2)}(kr) P_n^1(\cos \theta) \tag{11}$$

For simplicity, the superscatterer shell is equally segmented into 4 layers with homogeneous and isotropic materials. In layer m ($m = 1, 2, 3, 4$), the total EM field is superposition of both incident and scattering fields.

$$\prod_e^i = j \frac{\cos \varphi}{k_m^2} \sum_{n=1}^\infty [a_n^m \hat{J}_n(k_m r_m) + b_n^m \hat{H}_n^{(2)}(k_m r_m)] j^{-n} P_n^1(\cos \theta)$$

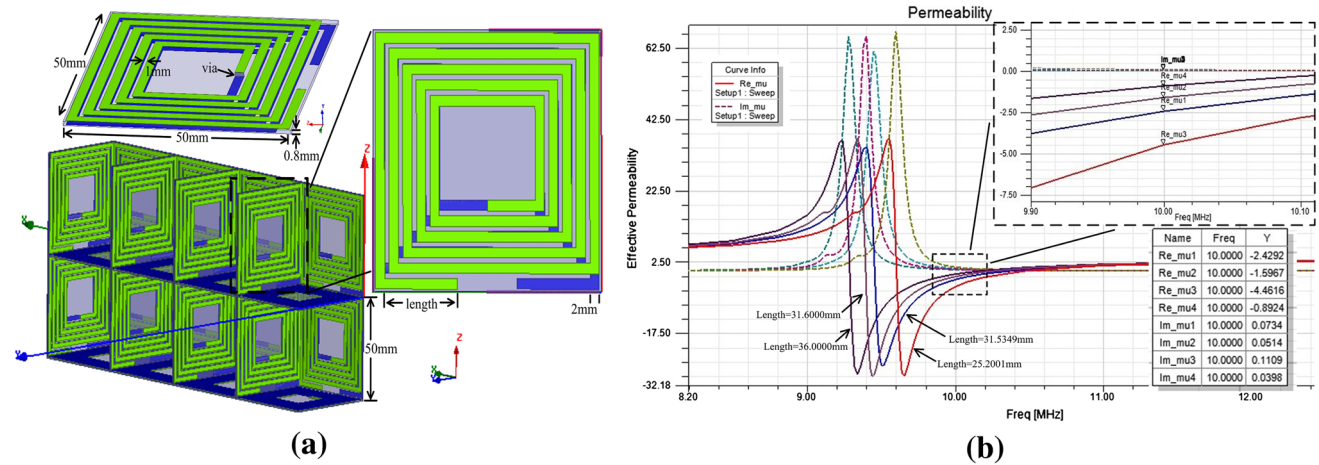
$$\prod_m^i = j \frac{\sin \varphi}{k_m^2 Z_m} \sum_{n=1}^\infty [d_n^m \hat{J}_n(k_m r_m) + c_n^m \hat{H}_n^{(2)}(k_m r_m)] j^{-n} P_n^1(\cos \theta) \tag{12}$$

The components of EM field $E_\theta, E_\varphi, H_\theta, H_\varphi$ can be expressed by Hertzian vectors from Eq. (12) in terms of coefficients a_n, b_n, c_n, d_n in different layers. Using the boundary conditions: $E_\theta^{m+1} = E_\theta^m, E_\varphi^{m+1} = E_\varphi^m, H_\theta^{m+1} = H_\theta^m$ and $H_\varphi^{m+1} = H_\varphi^m$, we can obtain the recurrence relation between $[a_n^{m+1}, b_n^{m+1}, c_n^{m+1}, d_n^{m+1}]$ and $[a_n^m, b_n^m, c_n^m, d_n^m]$. As for the innermost layer, the electric field on the surface of PEC boundary is zero. Therefore, the starting coefficients in the recurrence relation are:

$$b_n^1 = -a_n^1 \frac{\hat{J}_n'(k_1 R_1)}{\hat{H}_n^{(2)'}(k_1 R_1)}, \quad c_n^1 = -d_n^1 \frac{\hat{J}_n(k_1 R_1)}{\hat{H}_n^{(2)}(k_1 R_1)} \tag{13}$$

Table 2 Optimized permeability for 4-layered superscatterer (thickness of each layer is 0.125 m)

Layer	Layer 1	Layer 2	Layer 3	Layer 4
μ	-2.4292	-1.5967	-4.4616	-0.8924
$\mu(\text{loss})$	-2.4292 + 0.0734i	-1.5967 + 0.0514i	-4.4616 + 0.1109i	-0.8924 + 0.0398i

**Fig. 8** **a** Unit cell and periodic structure of metamaterials. **b** Effective permeability retrieved from magnetic metamaterials with different lengths

Using the recurrence relation and known condition in the air: $a_n = d_n = (2n + 1)/(n^2 + n)$, we can determine the scattering coefficients b_n, c_n in the air. Based on the definition of scattering width (SW) in Eq. (14), we can compare the SW of superscatterer with that of equivalent case.

$$\sigma_s(\theta) = \frac{2\pi}{k^2} \sum_{n=1}^{\infty} (2n + 1)(|b_n|^2 + |c_n|^2) \quad (14)$$

As the scattering coefficients b_n, c_n are influenced by wave number $k = \omega\sqrt{\epsilon\mu}$ and wave impedance $Z = \sqrt{\mu/\epsilon}$, the scattering width of superscatterer is dependent on permeability in each layer. Hence, we can establish an objective function between SW of superscatterer and that of equivalent case.

$$F_1(\mu_1, \mu_2, \mu_3, \mu_4) = \int_0^{\pi} [\sigma_s(\theta)|_{R1 < r < R2} - \sigma_s(\theta)|_{r=R3}]^2 d\theta \quad (15)$$

If the F_1 function reaches the minimum value, which means the scattering field of superscatterer agrees well with that of equivalent case, the 4-layered superscatterer will be a good approximation for rigorous one. To search optimal parameters, the genetic algorithm toolbox in MATLAB is employed. After computation, we get a set of permeability $[\mu_1, \mu_2, \mu_3, \mu_4]$ for 4 layers. However, these parameters still need to be adjusted by finer optimization process, because

the size of superscatterer is much smaller than EM wavelength which belongs to Rayleigh scattering. In this respect, these parameters are a coarse optimized result for near field.

To further optimize the permeability in each layer, we consider the self-inductance of coil and mutual inductance M of two coils. If the coil in superscatterer is equivalently expanded, its self-inductance should be the same as that of equivalent larger coil, which is reflected by magnetic energy because $E_m = Li^2/2$. If the coil in superscatterer is equivalently moved to a farther position, the mutual inductance should equal the M of shifted coil and the receiving one. So, another objective function in Eq. (16) is employed. Here, E_m^{scr} is the total magnetic energy of coil with superscatterer, which can be derived from global evaluation in COMSOL. $M^{scr}(d_i)$ is the mutual inductance between two coils with superscatterer when transmitting coil has a displacement d_i . The entire objective function is optimized by Nelder–Mead algorithm in COMSOL, and the coarse optimized result from Eq. (15) is used as initial seed to facilitate the search process of optimization. The final optimal parameters of 4-layered superscatterer are listed in Table 2 (first line).

$$F_2(\mu_1, \mu_2, \mu_3, \mu_4) = |E_m^{scr} - E_m^{eq}|^2 + \sum_i |M^{scr}(d_i) - M^{eq}(d_i)|^2 \quad (16)$$

Taking the final optimized permeability into 4-layered superscatterer and keeping the conditions the same as those in Sect. 3, the magnetic field of superscatterer is displayed in Fig. 7c and the mutual inductance is also evaluated and

plotted in Fig. 7d (yellow line with star markers). Clearly, both the magnetic field and mutual inductance agree well with those of rigorous superscatterer and equivalent case. That means, the 4-layered superscatterer with optimized permeability can mimic the rigorous superscatterer in a pretty good way. Moreover, the structure is much simpler than 10-layered superscatterer based on EMT.

The negative parameters in Table 2 are limited value which can be achieved by resonant magnetic metamaterials. For fabrication concerns, we make some slight changes on the unit cell proposed in previous paper [14], which is exhibited in Fig. 8a. The unit cell has a square shape with $50 \text{ mm} \times 50 \text{ mm}$ size. On both top and bottom layers, the spiral copper strip has five turns with 2 mm width and 1 mm spacing. The thicknesses of substrate and the copper strip are 0.8 and 0.035 mm, respectively. Rogers 6010 is selected as the material of substrate. Moreover, the length of outermost edge is variable for searching best parameters (see the 'length' marked in Fig. 8a). Finally, the unit cells are placed and assembled in periodic structure to form isotropic metamaterial.

The entire model is simulated by HFSS, and the effective permeability is retrieved based on S parameter method [26]. By sweeping the variable of length, we obtain a set of lengths to meet the requirement of effective permeability in Table 2. Both real and imaginary parts are plotted in Fig. 8b, and the value of permeability is marked at 10 MHz. The imaginary part reflects the magnetic loss of such metamaterial (see Table 2 second line), and the dielectric loss is reflected by the loss tangent of substrate materials. Considering the ohmic loss (reflected by imaginary part of permittivity), we take both complex permeability and permittivity value into the 4-layered superscatterer to evaluate the performance of layered superscatterer with losses. The mutual inductance is computed and plotted in magenta dotted line with 'plus' marker (see Fig. 7d). The result is still better than 10-layered superscatterer. Besides, the influence of frequency deviation is considered. We change the permeability according to the curves in Fig. 8b within the range of 9.99–10.01 MHz, which has a 20-kHz-wide band. The worst case is simulated, and mutual inductance is evaluated in black dash line with diamond markers (see Fig. 7d).

Compared with rigorous superscatterer and 10-layered superscatterer, the optimized 4-layered superscatterer is simpler and more practical, because its unit cell with loss is considered and it does not need active material. The fewer layers with homogeneous and isotropic material will reduce the difficulty of fabrication, and the tolerance of frequency deviation is also acceptable.

5 Conclusion

In conclusion, the influence of superscatterer without PEC boundary has been analyzed in this paper especially with

a source inside. The results indicate that such superscatterer can equivalently expand the size of original object and shift its position. The tensors of permittivity and permeability of EM media in region $r < R_1$ and $R_1 < r < R_2$ are also derived from transformation optics. By changing EM parameters and the position of object, we can achieve desired equivalent expansion and displacement of object. Moreover, both losses and impedance mismatch are considered and the effect of superscatterer still holds in inductive coupling system. We also discuss the possible simplification of proposed superscatterer for fabrication concerns. The unit cell of metamaterial and its effective permeability are presented. Numerical analysis shows the advantages of optimized 4-layered superscatterer, which is more feasible for practical engineering. The potential applications of such superscatterer are to shrink the size of EM device, to enlarge and shift the coils in WPT systems and to enhance coupling of NFC/RFID antenna system, which is partly analyzed in Sect. 3.

Acknowledgments This work is supported by National Natural Science Foundation of China (51277120) and the International S&T Cooperation Program of China (2012DFG01790).

References

1. J.B. Pendry, D. Schurig, D.R. Smith, Controlling electromagnetic fields. *Science* **312**(5781), 1780–1782 (2006)
2. D. Schurig, J.B. Pendry, D.R. Smith, Calculation of material properties and ray tracing in transformation media. *Opt. Express* **14**(21), 9794–9804 (2006)
3. S.A. Cummer, R. Liu, T.J. Cui, A rigorous and nonsingular two dimensional cloaking coordinate transformation. *J. Appl. Phys.* **105**(5) (2009)
4. H.Y. Chen, C.T. Chan, Transformation media that rotate electromagnetic fields. *Appl. Phys. Lett.* **90**(24) (2007)
5. F.M. Kong, et al., Planar focusing antenna design by using coordinate transformation technology. *Appl. Phys. Lett.* **91**(25) (2007)
6. D. Schurig et al., Metamaterial electromagnetic cloak at microwave frequencies. *Science* **314**(5801), 977–980 (2006)
7. G.W. Milton et al., A proof of superlensing in the quasistatic regime, and limitations of superlenses in this regime due to anomalous localized resonance. *Proc. R. Soc. Lond. Ser.* **461**(2064), 3999–4034 (2005)
8. X.D. Luo et al., Conceal an entrance by means of superscatterer. *Appl. Phys. Lett.* **94**(22) (2009)
9. W.H. Wee, J.B. Pendry, Shrinking optical devices. *New J. Phys.* **11** (2009)
10. T. Yang et al., Superscatterer: enhancement of scattering with complementary media. *Opt. Express* **16**(22), 18545–18550 (2008)
11. D.R. Smith et al., Composite medium with simultaneously negative permeability and permittivity. *Phys. Rev. Lett.* **84**(18), 4184–4187 (2000)
12. A. Rajagopalan et al., Improving power transfer efficiency of a short-range telemetry system using compact metamaterials. *IEEE Trans. Microw. Theory Tech* **62**(4), 947–955 (2014)
13. O.M. Ramahi, et al., Metamaterial particles for electromagnetic energy harvesting. *Appl. Phys. Lett.* **101**(17) (2012)

14. B.N. Wang, et al., Experiments on wireless power transfer with metamaterials. *Appl. Phys. Lett.* **98**(25) (2011)
15. J.B. Pendry, Negative refraction makes a perfect lens. *Phys. Rev. Lett.* **85**(18), 3966–3969 (2000)
16. D. Huang, et al., Magnetic superlens-enhanced inductive coupling for wireless power transfer. *J. Appl. Phys.* **111**(6) (2012)
17. J.B. Pendry, S.A. Ramakrishna, Focusing light using negative refraction. *J. Phys. Condens. Matter* **15**(37), 6345–6364 (2003)
18. X.H. Zhang et al., Transformation media that turn a narrow slit into a large window. *Opt. Express* **16**(16), 11764–11768 (2008)
19. M. Rahm et al., Design of electromagnetic cloaks and concentrators using form-invariant coordinate transformations of Maxwell's equations. *Photo. Nano. Fund. Appl.* **6**(1), 87–95 (2008)
20. H.Y. Chen, Transformation optics in orthogonal coordinates. *J. Opt. A Pure Appl. Opt.* **11**(7) (2009)
21. G.W. Milton, et al., Solutions in folded geometries, and associated cloaking due to anomalous resonance. *New J. Phys.* **10** (2008)
22. H.X. Xu et al., Superscatterer illusions without using complementary media. *Adv. Opt. Mater.* **2**(6), 572–580 (2014)
23. Y. Huang, Y. Feng, T. Jiang, Electromagnetic cloaking by layered structure of homogeneous isotropic materials. *Opt. Express* **15**(18), 11133–11141 (2007)
24. C.W. Qiu, et al., Spherical cloaking with homogeneous isotropic multilayered structures. *Phys. Rev. E.* **79**(4) (2009)
25. Z.Z. Yu, et al., Optimized cylindrical invisibility cloak with minimum layers of non-magnetic isotropic materials. *J. Phys. D Appl. Phys.* **44**(18) (2011)
26. D.R. Smith, et al., Determination of effective permittivity and permeability of metamaterials from reflection and transmission coefficients. *Phys. Rev. B.* **65**(19) (2002)